The DOI for this manuscript is doi: 10.1175/JPO-D-11-0238.1

The final published version of this manuscript will replace the preliminary version at the above DOI once it is available.

If you would like to cite this EOR in a separate work, please use the following full citation:

Greatbatch, R., P. Brandt, M. Claus, S. Didwischus, and Y. Fu, 2012: On the width of the equatorial deep jets. J. Phys. Oceanogr. doi:10.1175/JPO-D-11-0238.1, in press.

On the width of the equatorial deep jets

R. J. Greatbatch,* P. Brandt, M. Claus, S.-H. Didwischus and Y. Fu

GEOMAR | Helmholtz Zentrum für Ozeanforschung Kiel, Kiel, Germany

**Corresponding author address:* R. J. Greatbatch, GEOMAR | Helmholtz Zentrum für Ozeanforschung Kiel, Düsternbrooker Weg 20, 24105 Kiel.

E-mail: rgreatbatch@geomar.de

ABSTRACT

The equatorial deep jets (EDJ) are a striking feature of the equatorial ocean circulation. In the Atlantic Ocean, the EDJ are associated with a vertical scale of between 300 and 700 m, a time scale of roughly 4.5 years and upward energy propagation to the surface. It has been found that the meridional width of the EDJ is roughly 1.5 times larger than expected based on their vertical scale. Here we use a shallow water model for a high order baroclinic vertical normal mode to argue that mixing of momentum along isopycnals can explain the enhanced width. A lateral eddy viscosity of 300 m^2 s^{-1} is found to be sufficient to account for the width implied by observations.

1. Introduction

Equatorial deep jets (EDJ) were first discovered in the equatorial Indian Ocean (Luyten and Swallow 1976) and are now known to be a ubiquitous feature of the zonal flow along the equator in all three ocean basins. The jets appear as vertically alternating bands of eastward and westward flow with a vertical scale measured in hundreds of meters and velocities typically near 0.1 m s^{-1}. Brandt et al. (2011) have shown that in the equatorial Atlantic these jets exhibit quite regular behaviour associated with downward phase propagation (implying, according to linear theory, upward energy propagation) and a time scale of roughly 4.5 years (see also Johnson and Zhang 2003; Bunge et al. 2008). The 4.5 year signal can be seen in sea surface temperature (SST) as well as atmospheric data (e.g. surface wind and rainfall) indicating the significance of the deep jets for climate.

The similarity between the EDJ and the gravest equatorial basin mode (Cane and Moore 1981) for a high order baroclinic vertical normal mode has been noted by many authors, e.g. Johnson and Zhang (2003), D'Orgeville et al. (2007) and Brandt et al. (2011), although since the EDJ propagate vertically they cannot correspond exactly to such a mode (in reality there is forcing and dissipation as well as the influence of variable bottom topography and non-linearity to break an exact correspondence to a basin mode). The gravest basin mode has a time scale set by the time taken for an equatorial Kelvin wave to propagate from the western to the eastern boundary and then return as the gravest, long equatorial Rossby wave. For the time scale of 4.5 years identified by Brandt et al. (2011) for the Atlantic Ocean, the corresponding gravity wave speed is about 0.17 m s^{-1}, appropriate to roughly the 15th vertical normal mode (see Figure 11 in Brandt et al. (2008) who argue, based on the data available to them, that the zonal velocity variations associated with the deep jets are best respresented by a spread of vertical normal modes centred on the 15th mode). Nevertheless, a baffling feature of the EDJ is that their cross-equatorial width is found to be roughly 1.5 times larger than implied by their vertical structure based on inviscid, linear theory (Johnson and Zhang 2003), the topic we investigate in the present paper. The enhanced cross-equatorial width, again by a factor of 1.5, has also been noticed by Muench et al. (1994) in the case of the equatorial deep jets observed in the Pacific Ocean.

Here we exploit the similarity between the EDJ and an equatorial basin mode and use a linear shallow water model for a high order baroclinic vertical normal mode to demonstrate the dependence of the meridional width about the equator on the lateral (isopycnal) mixing of momentum. The underlying physics is discussed by Yamagata and Philander (1985) and can be understood by noting that for a baroclinic equatorial basin mode, the zonal flow along the equator is to a good approximation in geostrophic balance. Reducing the strength of this flow by fluxing momentum away from the equator requires, by thermal wind, a reduced meridional density gradient either side of the equator. In the absense of diapycnal mixing to remove the equatorial density perturbation supporting the flow, there is then a requirement for a larger meridional width than given by inviscid theory. Diapycnal mixing is known to be particularly weak near the equator[1] (Dengler and Quadfasel 2002; Gregg et al. 2003), with typical diapycnal diffusivities of order 10^{-6} m^2 s^{-1}, consistent with the above explanation. Brandt et al. (2008) have noted the importance of lateral mixing for closing the oxygen budget at the equator and used a value of 400 m^2 s^{-1} which, as we show, is sufficient to account for the enhanced cross-equatorial width of the deep jets. It is nevertheless possible

[1] At least below the region of strong vertical shear associated with the Equatorial Undercurrent.

that other mechanisms play a role. For example, Hua et al. (1997) have suggested that nonlinearity induced by the strong zonal currents might lead to a broadening of the jets about the equator.

Since the EDJ have much larger zonal than meridional scale, we expect lateral mixing of momentum to be associated with fluctuations in the meridional velocity that occur on much shorter time scales than the time scale of 4.5 years associated with the EDJ themselves. Such meridional velocity fluctuations are readily found in observations from moorings deployed at the equator, typically with a time scale of 10's of days and often associated with Yanai waves (see, for example, Muench et al. (1994), Figures 3 and 4 in Bunge et al. (2008) and Figure 2 in von Schuckmann et al. (2008)).

In the model to be described below, we apply an oscillatory forcing to balance the dissipative effect of the lateral mixing of momentum. Here we choose simple forms, i.e. forcing only for the zonal momentum equation and forcing that is either spatially uniform within the regions it is applied (to avoid biasing the cross-equatorial width of the modelled jets) or is focussed on the equator to mimic the possibility that the EDJ are maintained by processes that take place within the equatorial wave guide. Exactly how the EDJ are maintained against dissipation in reality is a topic of ongoing research. Various mechanisms have been suggested, recent examples involving the destabilization of Yanai waves (Hua et al. 2008) excited either by fluctuations of the deep western boundary current (D'Orgeville et al. 2007; Eden and Dengler 2008; Ménesguen et al. 2009a) or by instabilities of the surface flow, e.g. tropical instability waves (Ménesguen et al. (2009a), Ascani, personal communication[2]). In-

[2] Ascani et al. (2010) show that downward propagating Yanai waves, generated by tropical instability waves and that break at depth, are able to generate the quasi-steady flanking jets with large vertical scale

terestingly, Muench and Kunze (1999) and Muench and Kunze (2000) have suggested that momentum transfer into the EDJ due to critical layer interactions involving gravity waves could be important, a mechanism in which small scale processes inject momentum into the EDJ rather than remove it. Here we are not concerned with the details of the mechanism; we simply impose a forcing to counter the dissipation and allow the model to achieve a steady, oscillating state. However, we can use the shallow water model to test regions where applied forcing can more efficiently excite a dissipative basin mode, an issue we explore briefly in this paper.

The plan of the paper is as follows. Section 2 provides the model description. In Section 3 the model results are presented together with a comparison between the model results and an analysis of both ARGO float data (Lebedev et al. 2007) and cruise data (the cruises are listed in Table 1). Section 4 provides a summary and discussion.

2. The model

We work with a shallow water model for the horizontal structure associated with a high order baroclinic vertical normal mode (see Gill 1982), the governing equations of which are given in spherical coordinates by

$$u_t - fv = -\frac{g}{a\cos\theta}\frac{\partial\eta}{\partial\lambda} + X + F^u \tag{1}$$

associated with the Equatorial Intermediate Current system. It is important to note that these flanking jets are different from the EDJ. The latter, the main topic of this paper, have much smaller vertical scale and exhibit quasi-periodic behaviour.

$$v_t + fu = -\frac{g}{a}\frac{\partial \eta}{\partial \theta} + F^v \tag{2}$$

$$\eta_t + \frac{H}{a\cos\theta}\left[\frac{\partial u}{\partial \lambda} + \frac{\partial(\cos\theta v)}{\partial \theta}\right] = 0 \tag{3}$$

where θ is latitude, λ is longitude, a is the radius of the Earth, g is the acceleration due to gravity, $f = 2\Omega \sin\theta$ is the Coriolis parameter, H is the equivalent depth, u, v the horizontal velocity components in the eastward and northward directions, respectively, η corresponds to the isopycnal displacement, and $X = X_o sin(\omega t)$ is the oscillatory forcing we use to counter the dissipation. (F^u, F^v) is the lateral mixing of momentum with eddy viscosity, A, given by

$$F^u = A\left[\nabla^2 u + \frac{u(1-tan^2\theta)}{a^2} - \frac{2sin\theta}{a^2cos^2\theta}\frac{\partial v}{\partial \lambda}\right], \tag{4}$$

$$F^v = A\left[\nabla^2 v + \frac{v(1-tan^2\theta)}{a^2} + \frac{2sin\theta}{a^2cos^2\theta}\frac{\partial u}{\partial \lambda}\right] \tag{5}$$

and ∇^2 is the Laplacian operator given by

$$\nabla^2\gamma = \left[\frac{1}{a^2cos^2\theta}\frac{\partial^2\gamma}{\partial\lambda^2} + \frac{1}{a^2cos\theta}\frac{\partial}{\partial\theta}\left(cos\theta\frac{\partial\gamma}{\partial\theta}\right)\right]. \tag{6}$$

These equations are integrated using the method of Heaps (1971) applied to an idealised rectangular domain (in latitude/longitude space) of width 55° longitude, similar to that of the equatorial Atlantic, and extending from 10°S to 10°N. A free slip boundary condition is applied to the lateral viscosity term on all the boundaries and sponge layers are applied to the northern and southern boundaries to prevent Kelvin wave propagation along these boundaries (cf. Yang and Liu 2003). The equivalent depth H is chosen so that the gravity wave speed $c = \sqrt{gH} = 0.17$ m s^{-1} for which the corresponding period of the gravest basin mode ($\frac{4L}{c}$ where L is the basin width) is $T_B = 1670$ days (the same period that is identified by Brandt et al. (2011)). The horizontal resolution is 1/10° in latitude and longitude, sufficient to resolve the equatorial radius of deformation ($\sqrt{c/\beta} = 0.8°$).

3. Results

a. Model results

The analytic basin mode solutions in Cane and Moore (1981) are for an ocean with no forcing and dissipation. As noted earlier, to counter the dissipation when the eddy viscosity, A, is non-zero, we run the model using a zonal forcing (given by $X = X_o sin(\omega t)$ in (1)) that oscillates in time. For each specification of the forcing and the eddy viscosity, the model is run to a steady oscillating state.

We begin with a forcing that is spatially uniform and force the model using different oscillation periods (associated with the angular frequency ω), the same forcing amplitude[3], X_o, in each experiment and a value of $A = 10$ m^2 s^{-1}. Figure 1 shows the square root of the zonal/time average of the square of the zonal velocity along the equator in the final, steady oscillating state (the time average is taken over the final complete oscillation cycle). A resonance at the period of the gravest basin mode, 1670 days, is clearly evident and there is also a second resonance at the period of the second basin mode, near 835 days, corresponding to twice the frequency of the gravest mode.

[3]Note that since the model is linear, the value used for the amplitude is not important.

We now keep the amplitude of the (still spatially uniform) forcing fixed, the oscillation period fixed at 1670 days, and run the model to a steady oscillating state for a range of different values of the eddy viscosity A. For the different values of A, we compute, as a function of latitude, the square root of the zonal/time average of the square of the zonal velocity, averaged over the final cycle of each model run. The zonal average is carried out over the longitude range between 15° and 30° from the western boundary of the basin. The choice of longitude band used for the averaging is not especially important as long as the boundary layers at the eastern and western ends of the basin are avoided; here the longitude band is chosen to correspond to the same longitude band used for processing the ARGO float data, the choice being determined by the availability of the data (see Section 3b). To measure the width, L_e, of the model response about the equator, we use the meridional distance over which this quantity decreases to $\frac{1}{e}$ of its maximum value on the equator. L_e is plotted in Figure 2 as a function of A (the case denoted "Full" and plotted with solid circles) from which it is clear that the width about the equator increases as A increases, as expected. A scale analysis, applied to the shallow water equations and derived in the Appendix, can be used to obtain an expression for the functional dependence of L_e on A and is given by

$$L_e = \sqrt{\frac{c}{3\beta} + \sqrt{\left(\frac{c}{3\beta}\right)^2 + 4AT\frac{c}{3\beta}}} \tag{7}$$

where T is a time scale. The basic ingredients used to derive (7) are (i) geostrophic balance of the zonal flow along the equator expressed through the dependence on $\frac{c}{\beta}$ and (ii) the influence of the Laplacian eddy viscosity A which spreads the velocity signal away from the equatorial wave guide a distance $\sqrt{AT}$ during the time T. It is easily found that a good fit to the model results (case "Full" in Figure 2) is obtained by taking T equal to one third of the basin mode period[4]. Using this choice for T, the theoretical width, as given by (7), is also plotted in Figure 2, from which it is clear that (7) captures the functional dependence of L_e on A, despite the fact that only the time scale T in (7) has been fitted to the model results. The factor 3 that appears in combination with β in (7) arises from the dominance of the gravest Rossby wave (see Figure 4 and note that in both the cases shown, the phase propagation indicated along the equator is westward.). Johnson and Zhang (2003) have noted that the gravest Rossby wave also dominates the structure of the observed EDJ's.

Johnson and Zhang (2003) (their Figure 6) find that the cross-equatorial width of observed EDJs in the Atlantic is about 1.5 times larger than the cross-equatorial width of the gravest Rossby wave, where the width of the Rossby wave is that given by inviscid theory for the vertical mode that best fits the observed vertical structure. We can follow the same procedure to compute the cross-equatorial width for the gravest Rossby wave as is used to determine L_e for the model results shown in Figure 2. Doing so gives a value of $L_e = 0.65°$ for our model parameters - almost the same as given by (7) when $A = 0$ m^2 s^{-1}, i.e. $\sqrt{2c/3\beta}$. For a width of $1.5 \times 0.65° = 0.98°$, the corresponding value of A taken from Figure 2 based on both (7) and case "Full" is near 175 m^2 s^{-1}.

We have also run the model with the forcing, X, confined to either the eastern third, the centre third or the western third of the basin ("East", "Centre" and "West" respectively in Figure 2) but still with the same amplitude and oscillating in time with the basin mode period $T_B = 1670$ days, exactly as before. The greater width of the model response in "West" and "Centre" reflects a more important role for the Kelvin wave in these cases compared to

[4]The time scale T should not be confused with the time interval used for the averaging. The latter is always a complete oscillation period and is carried out when the model is in a steady, oscillating state.

the “East” and “Full”cases in which the Rossby wave dominates. Also shown in Figure 2 is a case (“Equator”) in which the forcing (X in (1)) is given by

$$X = X_o e^{-\frac{\beta y^2}{2c}} sin(\omega t), \tag{8}$$

where $y = a\theta$ (θ in radians), and hence is uniform in the zonal direction but confined within an equatorial Rossby radius of deformation of the equator, $\omega = 2\pi/T_B$ and X_o is the same amplitude as used for the previous experiments. For larger values of A in this experiment, there is a notable weakening of the dependence on A of the width, L_e. Indeed, a width, L_e, that is $1.5 \times 0.65°$ gives a value of A near 300 m^2 s^{-1} and therefore not greatly removed from the value of 400 m^2 s^{-1} used by Brandt et al. (2008) to close the oxygen budget along the equator. A value of $A = 400$ m^2 s^{-1} corresponds to a width of roughly $1.6 \times 0.65° = 1.02°$. Figure 2 also includes the case “Eq. half width” for which

$$X = X_o e^{-\frac{\beta y^2}{8c}} sin(\omega t) \tag{9}$$

so that the forcing is even more confined near the equator than in “Equator” (the cross-equatorial e-folding scale is half a radius of deformation). The weakened dependence of the width on A is even more apparent in this case and it is clear that even the largest value of A we consider (i.e. 600 m^2 s^{-1}) is insufficient to increase the width of the jets to 1.5 times 0.65°. This experiment is important because it argues that in the real world, the forcing for the jets is very unlikely to be this narrow.

Looking at Figure 2 we see a divergence of the different curves as we approach $A = 0$ m^2 s^{-1}. This is because many different Rossby waves (not only the gravest) increasingly come into play as the lateral eddy viscosity, A, is reduced to zero, complicating the interpretation of the width in this limit. For example, there is a strong focussing in the centre of the basin on the equator - and hence a very narrow cross-equatorial width - even for the case with $A = 10\ \mathrm{m}^2\ \mathrm{s}^{-1}$, as can be seen in Figure 4. Rossby wave focussing is a feature of the analytic solutions shown in Cane and Moore (1981) and is a consequence of the beta-dispersion of Rossby waves described by Schopf et al. (1981).

Figure 3 shows the square root of the zonal/time average of the square of the zonal velocity along the equator as a function of A for each case (the maximum amplitude of the forcing is the same in each model run). Here the zonal averaging is taken across the whole basin and the time averaging is taken over the final cycle of the model run (when the model is in a steady oscillating state). From this figure, it is clear that the amplitude of the model response is largest in the case when the forcing is spatially uniform, closely followed by the case in which the forcing is confined near the equator (but still zonally uniform). It is also clear that forcing in the centre of the basin leads to a larger amplitude than forcing in the western or eastern third, with the smallest amplitude found when the model is forced in the eastern third of the basin. In all cases, however, the amplitude decreases as the eddy viscosity, A, increases, as we expect. These results suggest that forcing in the centre of the basin is probably the most efficient way to excite a basin mode and that forcing in the eastern part of the basin is the most inefficient location. In reality, forcing via destabilizing Yanai waves excited by the deep western boundary current would be expected to provide a forcing in the western part of the basin whereas destabilizing Yanai waves generated by tropical instability waves could lead to forcing in almost any longitude band. Similar results (not shown) were obtained when the forcing was applied only over each of 6 equal widths spanning the basin, including when the forcing is confined near the equator as in Equation

(8).

b. Comparison with observations

In this subsection, we compare the model results to observations beginning with the available ARGO float data (Lebedev et al. 2007). The parking depth is around 1000 m (1000 m happens to be in the depth range where the EDJ have their largest amplitude). The first measurements are from August 1997 and the last from October 2011. We work in the longitude band 15°W to 30°W since this is where the ARGO float data are most plentiful (see Figure 4 in Brandt et al. (2011)). The data were binned into overlapping latitude bands of width 0.5° centered on a 0.25° zonal grid from 5°N to 5°S. A 1670 day harmonic was then fitted to the time series at each grid point. In Figure 5 the square of the resulting amplitude of the harmonic fit is shown at each grid point for the zonal velocity. The error bars show the estimated error of the harmonic fit with the assumption that all measurements are independent (in reality there is some autocorrelation, the effect of which is to increase the error bars).

We have also analysed deep velocity data from the cruises listed in Table 1, four of which collected data along 23° W down to 4000 m or deeper (Thalassa in August 1999, Meteor in April 2000, Meteor in November 2009 and Maria S. Merian in May/June 2011, where the name refers to the name of the research vessel). Vertical normal modes were computed from the mean density profile of the upper 4000 m from the different cruises and the zonal velocity was then projected onto these vertical normal modes[5]. From the four sections, we found the

[5] If the water depth was less than 4000 m, as was the case for a few stations along the section, the observed

maximum mean modal energy associated with the deep jets to be at the 17th vertical normal mode, for which the gravity wave speed $c = 0.16$ m s^{-1} (very close to the 0.17 m s^{-1} used in the model). Figure 6 shows the projection of the zonal velocity on to this mode as a function of latitude. Note that the data collected in 1999, 2000 and 2009 correspond to a similar phase of the 4.5 year cycle and all show projections of the same sign. The 2011 case, on the other hand, occurred when the phase of the 4.5 year cycle had changed leading to the opposite sign of the projection from the 1999, 2000 and 2009 cases.

Figure 7 shows cross-equator profiles of the model response for different values of A for the case that uses forcing confined near the equator (case "Equator" in Figure 2). The model response is the zonal/time average of the square of the zonal velocity, the zonal average being taken over the longitude band between 15° and 30° from the western boundary of the model domain (to correspond to the longitude range used for the analysis of the ARGO data) and the time average is over the last complete cycle of the model experiment (at a time when the model is in a steady oscillating state). For comparison, the figure also shows the cross-equator profile derived from the ARGO float data that is shown in Figure 5 (this time with no errors bars) and also the average of the cruise data shown in Figure 6 (here the projections in Figure 6 have been squared and then averaged to produce the profile shown in Figure 7). The curves (both model and observations) are normalised so that the area under each curve between 1° latitude either side of the equator is the same in each case. Near the equator, the ARGO float data show a strong bias to the north side of the equator (the bias is much reduced in the cruise data) although beyond 0.5° of the equator, the profiles are more symmetric. The symmetry of the model profiles is a consequence of using forcing

---

velocity field was extended down to 4000 m depth using zero velocity.

that is symmetric in latitude about the equator[6]. Comparing the model curves with the ARGO float data between $1°$ and $0.5°$ of the equator leaves the impression that the model agrees best with the observations for values of A between 100 m^2 s^{-1} and 300 m^2 s^{-1} on the southern side of the equator and between 300 m^2 s^{-1} and 600 m^2 s^{-1} on the northern side of the equator. The large value of up to 600 m^2 s^{-1} on the northern side of the equator is a consequence of the weak dependence of the cross-equatorial width on A, noted when discussing Figure 2, for values of A greater than about 200 m^2 s^{-1}. However, given the error bars on the profile from the ARGO float data (Figure 5) it is clear that a wide range of eddy viscosities, A, are compatible with the observations, although the case with the smallest value (A = 10 m^2 s^{-1}) is hard to reconcile with the observations. This latter conclusion is reinforced by the cruise data which are clearly not compatible with the A = 10 m^2 s^{-1} case. The cruise data profile also extends further away from the equator on the south side, favouring a fit to larger values of A than the ARGO data. Put together, these results are broadly consistent with our previous findings, indicating that a value of A of 300 m^2 s^{-1} is sufficient to account for the observed cross-equatorial width of the deep jets.

c. *Possible influence of the background, quasi-steady flow*

Figure 8a shows the mean zonal flow along $23°$ W, where the mean here refers to the average over all the cruises listed in Table 1 (Figure 8a is an update of the corresponding panel shown in Figure 2 of Brandt et al. (2010), including here the deep flow down to the

[6]Of course, it is possible that the asymmetry seen in the ARGO data is a consequence of asymmetry in the forcing that is producing the observed jets, a topic that is beyond the scope of the present paper.

bottom). Particularly striking are the eastward jets near 2°N and 2°S. These jets extend all the way to the bottom, have much larger vertical structure than the few hundred metres associated with the EDJ, and are the topic of the papers by Fruman et al. (2009) and Ascani et al. (2010) who attribute their existence to the destabilisation (Fruman et al.) or breaking (Ascani et al.) of Yanai waves generated in Ascani et al. by the instability of the surface equatorial current system (see also Ménesguen et al. (2009a)). The question arises as to whether these flanking jets can influence the EDJ?

The first point to note is that, in contrast to the EDJ, the flanking jets are quasi-steady phenomena. Indeed, the reason the flanking jets do not appear in Figure 5 is because a 1670 day harmonic fit is used to create Figure 5 and there is no projection of the flanking jets on to this fit. Since in our study, the lateral eddy viscosity, A, is taken to be a time-independent constant, it follows that there can be no direct influence of the flanking jets on the EDJ in our model set-up. Nevertheless, it is possible that the small scale velocity fluctuations responsible for the lateral mixing of momentum parameterised using A depend on the presence of the flanking jets, for example due to instabilities arising from the interaction between the jets and the EDJ. It is also possible that the lateral eddy viscosity, A, should vary spatially, depending on the background mean flow; the flanking jets could in fact act as a barrier to lateral mixing as suggested by Ménesguen et al. (2009a). While we recognise this possibility, it should be noted that it is only for very large values of A (see Figure 2) that the modelled EDJ impinge significantly on the flanking jets. It follows that the flanking jets are at the outer limit of the range of widths being considered here, corresponding only to the largest values of A when, in fact, the dependence of the cross-equatorial width on A is already weak (as noted when discussing Figure 2). Hence, while the flanking jets may indeed act as a barrier to lateral mixing, we argue that it is the lateral mixing within the region bounded by the flanking jets that is important.

Secondly, since the EDJ are associated with much higher (baroclinic) vertical normal modes than the flanking jets but, nevertheless, like the flanking jets extend to considerable depth, one way to assess the impact of the flanking jets is to compute the gradient of the absolute vorticity field shown in Figure 8b and compare this to the gradient of the planetary vorticity, $\beta = 2.3 \times 10^{-11}$ m^{-1} s^{-1}. The influence of the flanking jets is clearly seen in the figure, especially on the south side of the equator where there is a tendency between 2°S and 1°S for the gradient to be reduced compare to β. This reduction might be a factor in determining the northward bias in the EDJ between 1°S and 1°N noted when discussing Figure 7. The most striking feature, however, is the vertical band of enhanced values of the gradient near 2°S. This band of enhanced gradient might be related to the larger amplitude of the side lobe in the EDJ at this latitude compared to the corresponding feature on the north side of the equator (see Figure 5). Both these issues are topics for further investigation. Overall, however, the plot suggests that our analysis using a linear shallow water model for a high order baroclinic vertical normal mode is a reasonable first approximation for the EDJ between 1°S and 1°N. One further point to note is that the plot shown here is derived from an averaged representation of the background flow field. Instantaneously, it is possible that the absolute vorticity gradient could occasionally become negative, especially south of the equator, indicating the potential for barotropic instability. Variability arising from barotropic instability could be contributing to the lateral momentum mixing represented in our model by the lateral eddy viscosity, A. Finally we note that some authors have noted that the westward flowing bands of the EDJ are prone to inertial instability (Hua et al.

(1997), Ménesguen et al. (2009b); see also Fruman et al. (2009) for another example related to the dynamics of the flanking jets). Such instability might also be a source of mixing associated with the lateral eddy viscosity being invoked here.

4. Summary and discussion

We have used a linear shallow water model to simulate a forced, dissipative equatorial basin mode for a high order baroclinic vertical normal mode which, in turn, we have taken to be a simple model for the equatorial deep jets (EDJ). We have shown that lateral mixing of momentum leads to a significant broadening of the basin mode structure about the equator (see Figure 2). We suggest that the same mechanism plays a role in explaining the enhanced cross-equatorial width of the EDJ compared to that implied by their vertical structure based on inviscid theory, a property of the EDJ that has been noted by Johnson and Zhang (2003) in the Atlantic Ocean and Muench et al. (1994) in the Pacific Ocean. Our attempt to compare the model solutions with the available observations suggests that a value of A of 300 m^2 s^{-1} is sufficient to explain the observed cross-equatorial width of the EDJ. Based on a budget for oxygen along the equator, Brandt et al. (2008) estimated a lateral diffusion coefficient of 400 m^2 s^{-1}, a value that is broadly consistent with the above, especially given the weak dependence of width, L_e, on A in the case that is forced only near the equator ("Equator" in Figure 2). The model results also argue that the forcing for the deep jets cannot be as narrow as half a radius of deformation for the dominant vertical mode since then unrealistically large values for the lateral mixing coefficient would be required to explain the observed cross-equatorial width of the EDJ.

These results point to the importance of lateral mixing of momentum for explaining the cross-equatorial width of the EDJ. Further work is required to assess the role of other processes. For example, a typical observed flow speed in the EDJ is 0.1 m s^{-1}, a significant fraction of the shallow water gravity wave speed for the corresponding vertical normal mode (here taken to be 0.17 m s^{-1}), and pointing to the need to investigate nonlinear processes. We also noted that since the EDJ propagate vertically, they cannot correspond exactly to a basin mode. In reality, different vertical modes must be excited and energy transferred between the different vertical modes. However, given that our simple theory applies to all vertical modes, our suggestion concerning the role of lateral mixing of momentum nevertheless remains valid. The interaction of the EDJ with the (barotropic) flanking jets, briefly discussed in Section 3c, also deserves further study.

As noted earlier, Muench et al. (1994) point out that the equatorial deep jets in the Pacific Ocean are, like those in the Atlantic, wider across the equator than implied by their vertical structure according to inviscid linear theory (in fact, wider by the same factor 1.5 as found by Johnson and Zhang (2003) in the case of the Atlantic EDJ). These authors attribute the enhanced width to the effect of Eulerian averaging of the cross-equatorial advection of the jets by meridional flows associated with mixed Rossby-gravity (i.e. Yanai) waves, a possibility that cannot be ruled out in the Atlantic Ocean also. One possibility is that our lateral eddy viscosity, A, is simply mimicing the effect of such meridional flows. There is, nevertheless, an important difference between the two processes, that noted by Muench et al. (1994) and that suggested here. In Muench et al. (1994), the process described is entirely reversible whereas a lateral eddy viscosity, by its nature, implies a loss of energy from the mean flow (here the EDJ) to smaller (horizontal) scale motions (for example, other equatorial waves). In our defense, we note that the oxygen budget analysis of Brandt et al. (2008) has already suggested that lateral mixing of similar magnitude to that invoked here is important near the equator. A broadened jet, such as envisaged by Muench et al. (1994), must also be a solution of the Eulerian averaged equations of motion. To maintain an averaged flow that is broader than implied by inviscid theory then requires a forcing term in the Eulerian averaged equations that must come from the divergence of the Reynolds stress in the Eulerian averaged zonal momentum equation. We suggest that the divergence of the lateral mixing of momentum in our study (represented by F^u and F^v in (1) and (2), respectively) is a parameterisation for the necessary divergence of the Reynolds stress. Clearly, a very careful analysis of observed data and/or models is required to properly unravel these two effects, one reversible and one irreversible.

Acknowledgments.

We have used the YoMaHa'07 Lebedev et al. (2007) dataset of velocities derived from Argo float trajectories and provided by APDRC/IPRC. This study has been supported by the Deutsche Forschungsgemeinschaft as part of the Sonderforschungsbereich 754 'Climate Biogeochemistry Interactions in the Tropical Ocean' and by the German Federal Ministry of Education and Research as part of the co-operative project 'North Atlantic'. We are grateful to Marcus Dengler for helpful discussions and to two anonymous reviewers for their helpful comments.

APPENDIX

Scaling argument for the jet width

For simplicity we use the equations written on an equatorial β-plane (cf. Gill (1982)). These equations are a good approximation given that we are working in a limited range of latitudes centred around the equator. The (unforced) zonal momentum can then be written as

$$\left[-A\nabla^2 + \frac{\partial}{\partial t}\right] u - \beta y v = -g\frac{\partial \eta}{\partial x} \tag{A1}$$

Let U and P be scales for the variations of u and $-g\eta$, respectively, and L and L_e be horizontal length scales for variations in the zonal (L) and meridional (L_e) directions, respectively. We assume $\frac{L_e}{L} << 1$ and work at the equator (i.e. we put $y = 0$). From (A1) it follows that

$$[\frac{2A}{{L_e}^2} + \frac{1}{T}]U = \frac{P}{L} \tag{A2}$$

where a simple dependence in the meridional direction of $e^{-\frac{y^2}{L_e^2}}$ has been assumed (consistent with evaluating L_e from the model as an e-folding scale; note that the factor of 2 comes from evaluating the second derivative of $e^{-\frac{y^2}{L_e^2}}$ at $y = 0$). Since $\frac{L_e}{L} << 1$, we can make the long wave approximation to give

$$\beta y u = -g\frac{\partial \eta}{\partial y}. \tag{A3}$$

Differentiating (A3) with respect to y and putting $y = 0$ gives

$$\beta u = -g\frac{\partial^2 \eta}{\partial y^2} \tag{A4}$$

from which it follows that

$$\beta U = 2\frac{P}{L_e^2} \tag{A5}$$

again assuming an $e^{-\frac{y^2}{L_e^2}}$ dependence for η. Eliminating $\frac{P}{U}$ from (A2) and (A5) leads to

$$L_e^4 - \frac{2}{\beta}\frac{L}{T}L_e^2 - \frac{4AT}{\beta}\frac{L}{T} = 0. \tag{A6}$$

Since the model results are dominated by the westward propagation of the gravest Rossby wave (see Figure 4), and these waves propagate with speed $\frac{c}{3}$ (where $c = \sqrt{gH}$), we set

$$\frac{L}{T} = \frac{c}{3}. \tag{A7}$$

(A6) then becomes

$$L_e^4 - \frac{2c}{3\beta}L_e^2 - 4AT\frac{c}{3\beta} = 0 \tag{A8}$$

whose solution is

$$L_e = \sqrt{\frac{c}{3\beta} + \sqrt{\left(\frac{c}{3\beta}\right)^2 + 4AT\frac{c}{3\beta}}} \tag{A9}$$

as given by (7). When $A = 0$, (A9) reduces to

$$L_e = \sqrt{\frac{2c}{3\beta}}. \tag{A10}$$

This is the e-folding width for the gravest Rossby wave in the inviscid limit obtained using the same procedure as we apply to the model solutions (see the text immediately before (7)).

As we note in the text following equation (7), the best fit to the model results (for spatially uniform forcing) is given when T in (A9) equals one third of the basin mode period. It is clear from Figure 2 that this simple scaling is remarkably successful at capturing the functional dependence of the e-folding width, L_e, on the lateral eddy viscosity, A, despite that fact that only one parameter, T, has been fitted.

REFERENCES

Ascani, F., E. Firing, P. Dutrieux, J. P. McCreary, and A. Ishida, 2010: Deep equatorial ocean circulation induced by a forced - dissipated Yanai beam. *J. Phys. Oceanogr.*, **40 (5)**, 1118–1142, doi:10.1175/2010JPO4356.1.

Brandt, P., A. Funk, V. Hormann, M. Dengler, R. J. Greatbatch, and J. M. Toole, 2011: Interannual atmospheric variability forced by the deep equatorial Atlantic Ocean. *Nature*, **473**, 497–500, doi:10.1038/nature10013.

Brandt, P., V. Hormann, B. Bourlès, J. Fischer, F. A. Schott, L. Stramma, and M. Dengler, 2008: Oxygen tongues and zonal currents in the equatorial Atlantic. *J. Geophys. Res.*, **113 (C4)**, doi:10.1029/2007JC004435.

Brandt, P., V. Hormann, A. Körzinger, M. Visbeck, G. Krahmann, L. Stramma, R. Lumpkin, and C. Schmid, 2010: Changes in the ventilation of the oxygen minimum zone of the tropical North Atlantic. *J. Phys. Oceanogr.*, **40 (8)**, 1784–1801, doi:10.1175/2010JPO4301.1.

Bunge, L., C. Provost, B. L. Hua, and A. Kartavtseff, 2008: Variability at intermediate depths at the equator in the Atlantic Ocean in 2000-06: Annual cycle, equatorial deep jets, and intraseasonal meridional velocity fluctuations. *J. Phys. Oceanogr.*, **38 (8)**, 1794–1806, doi:10.1175/2008JPO3781.1.

Cane, M. A. and D. W. Moore, 1981: A note on low-frequency equatorial basin modes. *J.*

Phys. Oceanogr., **11 (11)**, 1578–1584, doi:10.1175/1520-0485(1981)011⟨1578:ANOLFE⟩2.0.CO;2.

Dengler, M. and D. Quadfasel, 2002: Equatorial deep jets and abyssal mixing in the Indian Ocean. *J. Phys. Oceanogr.*, **32 (4)**, 1165–1180, doi:10.1175/1520-0485(2002)032⟨1165:EDJAAM⟩2.0.CO;2.

D'Orgeville, M., B. L. Hua, and H. Sasaki, 2007: Equatorial deep jets triggered by a large vertical scale variability within the western boundary layer. *J. Mar. Res.*, **65 (1)**, 1–25, doi:10.1357/002224007780388720.

Eden, C. and M. Dengler, 2008: Stacked jets in the deep equatorial Atlantic Ocean. *J. Geophys. Res.*, **113 (C4)**, 1–12, doi:10.1029/2007JC004298.

Fruman, M., B. L. Hua, and R. Schopp, 2009: Equatorial zonal jet formation through the barotropic instability of low-frequency mixed Rossby-gravity waves, equilibration by inertial instability, and transition to superrotation. *J. Atmos. Sci.*, **66**, 2600–2619, doi:10.1175/2009JAS2913.1.

Gill, A., 1982: *Atmosphere-Ocean Dynamics*. Academic Press, New York, 662 pp.

Gregg, M. C., T. B. Sanford, and D. P. Winkel, 2003: Reduced mixing from the breaking of internal waves in equatorial waters. *Nature*, **422 (6931)**, 513–5, doi:10.1038/nature01507.

Heaps, N. S., 1971: On the numerical solution of the three-dimensional hydrodynamical equations for tides and storm surges. *Mem. Soc. R. Sci. Liege*, 143–180.

Hua, B. L., M. D'Orgeville, M. D. Fruman, C. Ménesguen, R. Schopp, P. Klein, and

H. Sasaki, 2008: Destabilization of mixed Rossby gravity waves and the formation of equatorial zonal jets. *J. Fluid Mech.*, **610**, 311–341, doi:10.1017/S0022112008002656.

Hua, B. L., D. W. Moore, and S. L. Gentil, 1997: Inertial nonlinear equilibration of equatorial flows. *J. Fluid Mech.*, **331**, 345–371, doi:10.1017/S0022112096004016.

Johnson, G. C. and D. Zhang, 2003: Structure of the Atlantic Ocean Equatorial Deep Jets. *J. Phys. Oceanogr.*, **33 (3)**, 600–609, doi:10.1175/1520-0485(2003)033⟨0600:SOTAOE⟩2.0.CO;2.

Lebedev, K. V., H. Yoshinari, N. A. Maximenko, and P. W. Hacker, 2007: Velocity data assessed from trajectories of Argo floats at parking level and at the sea surface. *IPRC Technical Note*, **4 (2)**.

Luyten, J. and J. Swallow, 1976: Equatorial undercurrents. *Deep-Sea Res. Oceanogr. Abstr.*, Elsevier, Vol. 23, 999–1001.

Ménesguen, C., B. Hua, M. Fruman, and R. Schopp, 2009a: Dynamics of the combined extra-equatorial and equatorial deep jets in the atlantic. *J. Mar. Res.*, **67 (3)**, 323–346, doi:10.1357/002224009789954766.

Ménesguen, C., B. Hua, M. Fruman, and R. Schopp, 2009b: Intermittent layering in the equatorial deep jets. *J. Mar. Res.*, **67 (3)**, 347–360, doi:10.1357/002224009789954748.

Muench, J., E. Kunze, and E. Firing, 1994: The potential vorticity structure of equatorial deep jets. *J. Phys. Oceanogr.*, **24**, 418–428.

Muench, J. and E. Kunze, 1999: Internal wave interactions with equatorial deep jets. part i: Momentum-flux divergences. *J. Phys. Oceanogr.*, **29 (7)**, 1453–1467.

Muench, J. and E. Kunze, 2000: Internal wave interactions with equatorial deep jets. part ii: Acceleration of the jets. *J. Phys. Oceanogr.*, **30 (8)**, 2099–2110.

Schopf, P. S., D. L. T. Anderson, and R. Smith, 1981: Beta-dispersion of low-frequency rossby waves. *Dyn. Atmos. Oceans*, **5 (3)**, 187–214.

von Schuckmann, K., P. Brandt, and C. Eden, 2008: Generation of tropical instability waves in the Atlantic Ocean. *J. Geophys. Res.*, **113 (C4)**, doi:10.1029/2007JC004712.

Yamagata, T. and S. G. H. Philander, 1985: The role of damped equatorial waves in the oceanic response to winds. *J. Oceanogr.*, **41 (5)**, 345–357, doi:10.1007/BF02109241.

Yang, H. and Z. Liu, 2003: Basin modes in a tropical-extratropical basin. *J. Phys. Oceanogr.*, **33 (12)**, 2751–2763.

List of Tables

TABLE 1. List of the cruises used to calculate the mean velocity section at 23°W shown in Figure 8.

Cruise	Section	max. depth (m)
Thalassa (Aug. 1999)	6°S-6°N; 23°W	6000
Seward Johnson (Jan. 2000)	6°S-4°N; 23°W	2000
Meteor 47/1 (Apr. 2000)	5°S-4°N; 23°W	5000
Meteor 55 (Oct. 2002)	0°N-10°N; 24°W	650
Polarstern ANT XXII/5 (June 2005)	20°S-20°N; 23°W	300
Meteor 68/1 (May 2006)	2°S-0.5°N; 23°W	500
Ron Brown (June 2006)	5°S-13.5°N; 23°W	1500
Meteor 68/2 (June-July 2006)	4°S-15.25°N; 23°W	1300
Ron Brown (June-July 2006)	5°N-14.5°N; 23°W	1500
Ron Brown (May 2007)	4°N-15.5°N; 23°W	1500
Maria S. Merian 08/1 (Apr. 2008)	7.5°N-14°N; 23°W	600
L'Atalante (Feb.-Mar. 2008)	2°S-14°N; 23°W	400
L'Atalante (Mar. 2008)	2°S-14°N; 23°W	1300
Maria S Merian 10/1 (Nov.-Dez) 2008	4°N-14°N; 23°W	1000
Polarstern ANT XXV/5 (Apr.-May 2009)	20°S-20°N; 23°W	250
Endeavour 463 (May 2009)	5°S-3°N; 23°W	725
Meteor 80/1 (Oct.-Nov. 2009)	6°S-15°N; 23°W	600
Polarstern ANT XXVI/1 (Oct.-Nov. 2009)	20°S-20°N; 23°W	250
Meteor 80/1 (Nov.2009)	6°S-15°N; 23°W	4500
Meteor 81/1 (Feb. 2010)	11.5°S-13°N; 22°W	1200
Polarstern ANT XXVI/4 (Apr.-May 2010)	5°S-13.5°N; 23°W	250
Maria S. Merian 18/2 (May 2011)	0°N-15°N; 23°W	2000
Maria S. Merian 18/2 (May-June 2011)	5°S-5°N; 23°W	5200

List of Figures

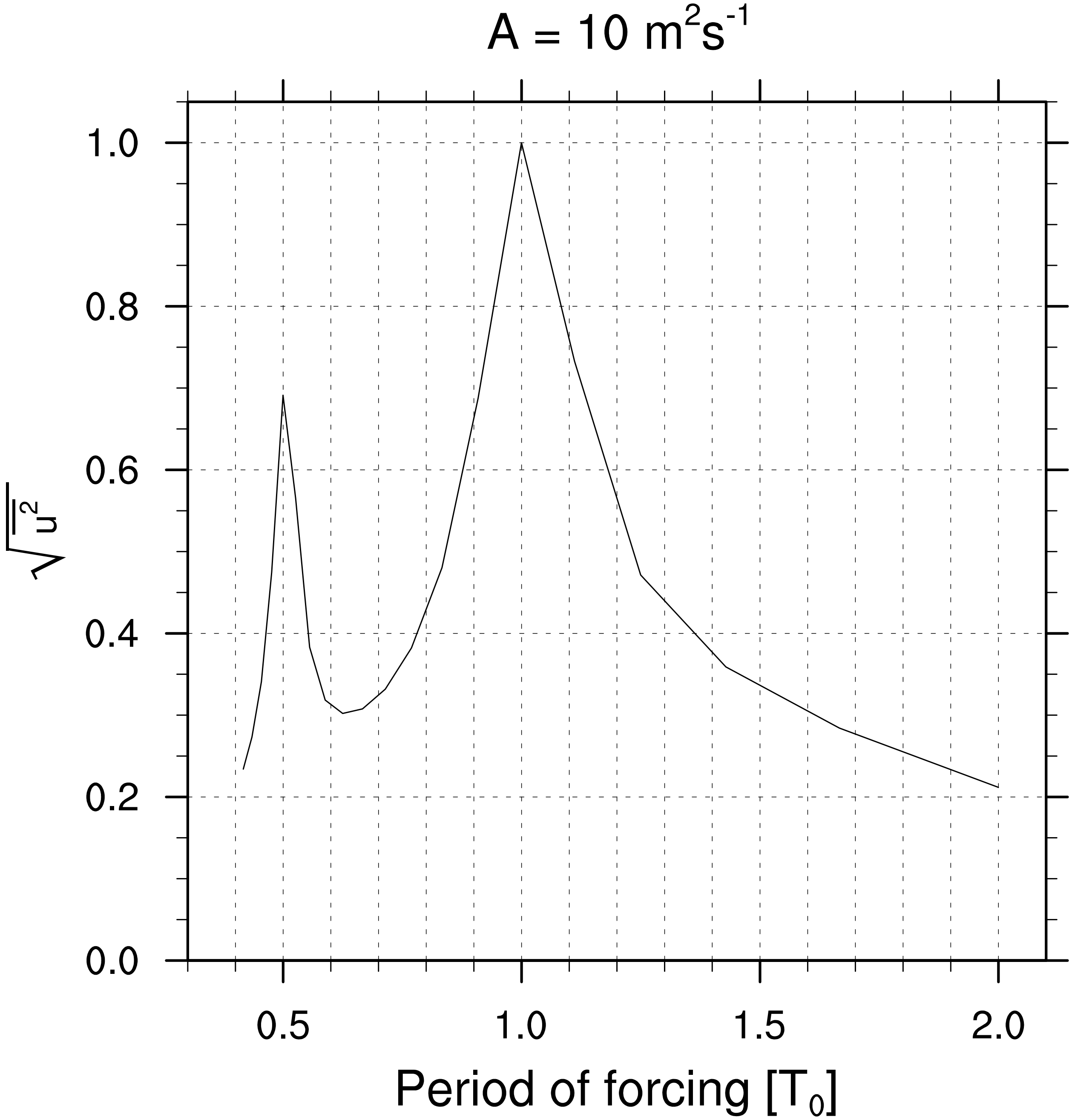

FIG. 1. The square root of the zonal/time average over the final cycle of the square of the zonal velocity along the equator as a function of the period T_o of the applied forcing. $A = 10$ m^2 s^{-1} and T_o is normalised by the period of the gravest basin mode, corresponding to $T_o = 1$ in the figure. The velocity in the ordinate is normalised by the maximum plotted amplitude.

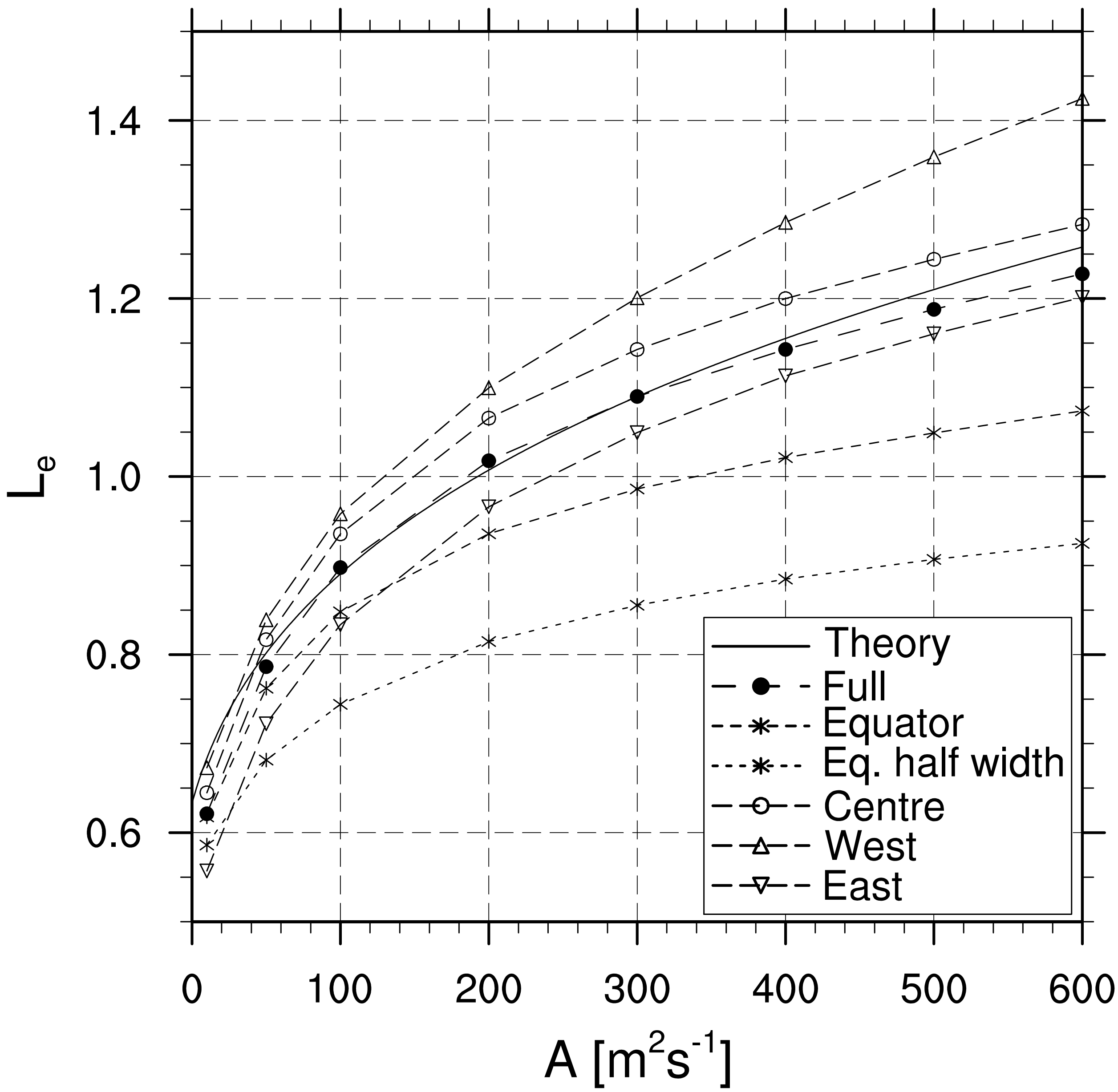

FIG. 2. The e-folding width (in degrees latitude) of the model response, L_e, about the equator and the theoretical prediction given by (7). In the different cases, the forcing is applied over the whole basin (Full), the centre third of the basin (Centre), the western third (West), the eastern third (East) or is zonally uniform but confined near the equator according to (8) (Equator) and (9) (Eq. half width).

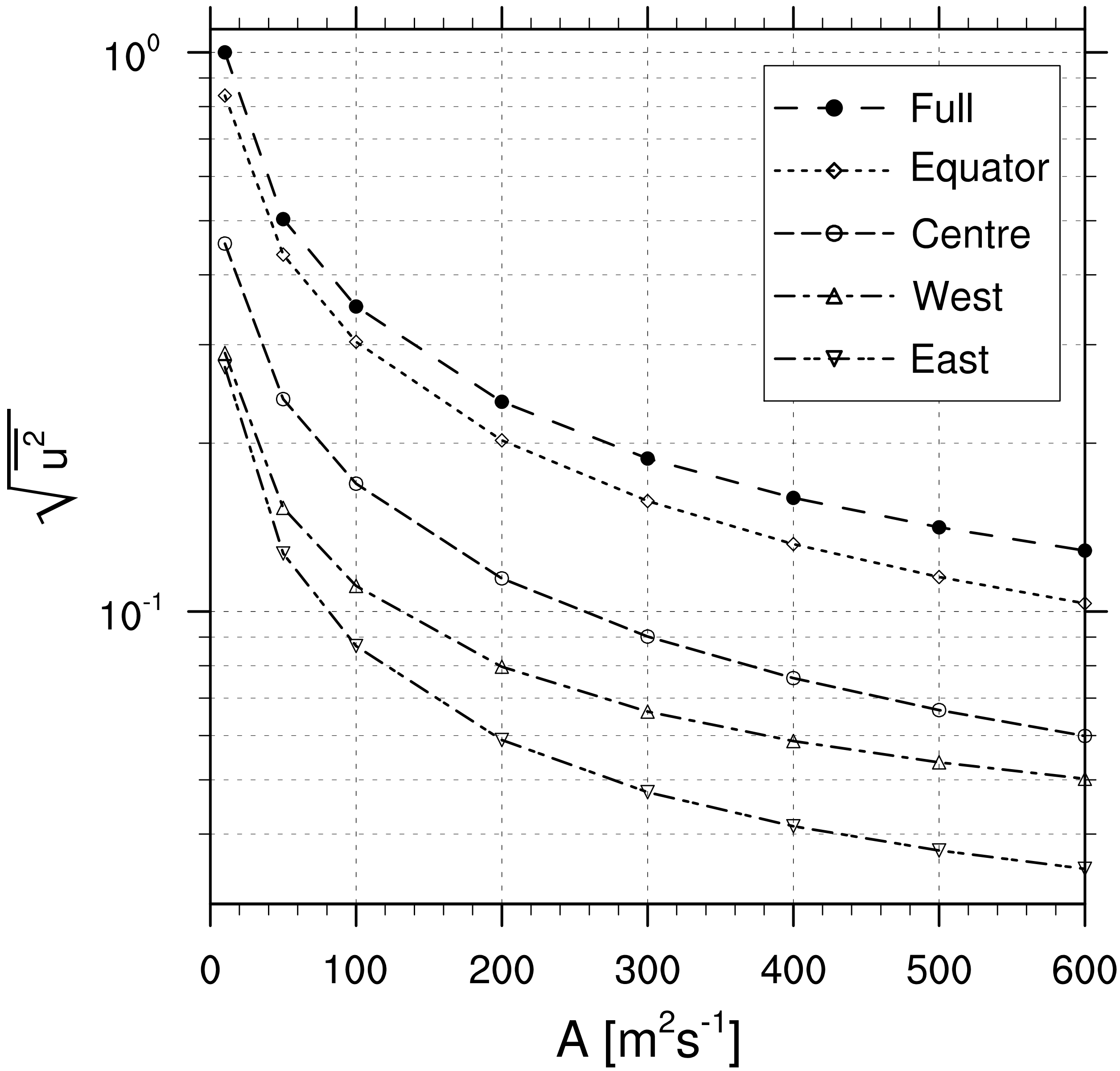

FIG. 3. The zonal/time average of the square of the zonal velocity along the equator as a function of A for cases with forcing applied over the whole basin (Full), the centre third of the basin (Centre), the western third (West), the eastern third (East) and when the forcing is zonally uniform but confined near the equator (Equator). The amplitude of the velocity shown by the ordinate is set by the choice of maximum forcing amplitude used for the model and is the same for all experiments. The numerical values appearing in the ordinate are normalised by the largest value shown.

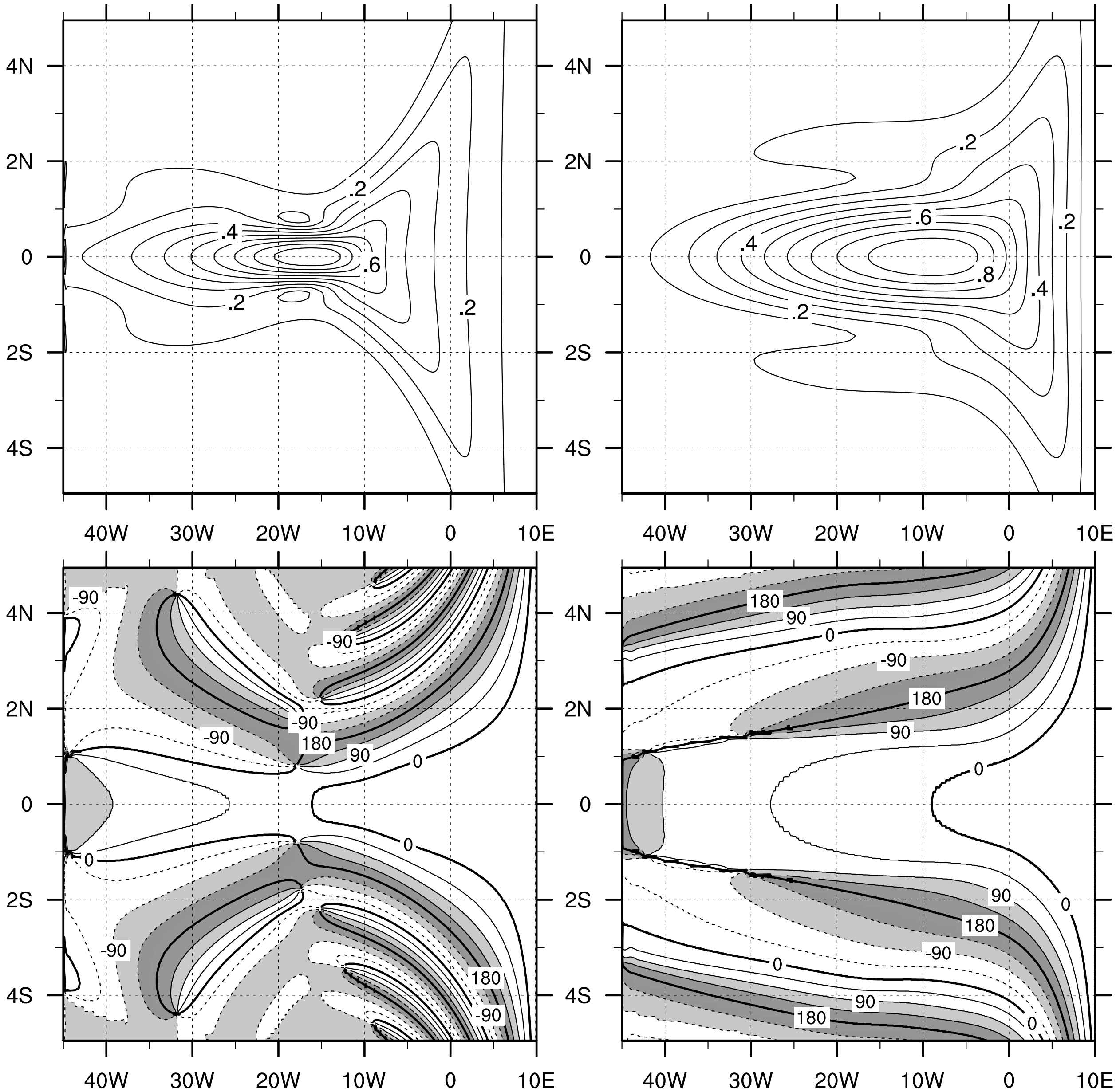

FIG. 4. The amplitude and phase of the model solution for $A = 10\ \mathrm{m^2\ s^{-1}}$ (left panels) and $A = 300\ \mathrm{m^2\ s^{-1}}$ (right panels) in cases corresponding to case "Full" in Figure 2. The amplitude is normalised with respect to the maximum amplitude in each plot and the phase is plotted with a contour interval of 45°, with positive phase indicating a lag compared to zero and dashed contours indicating negative values.

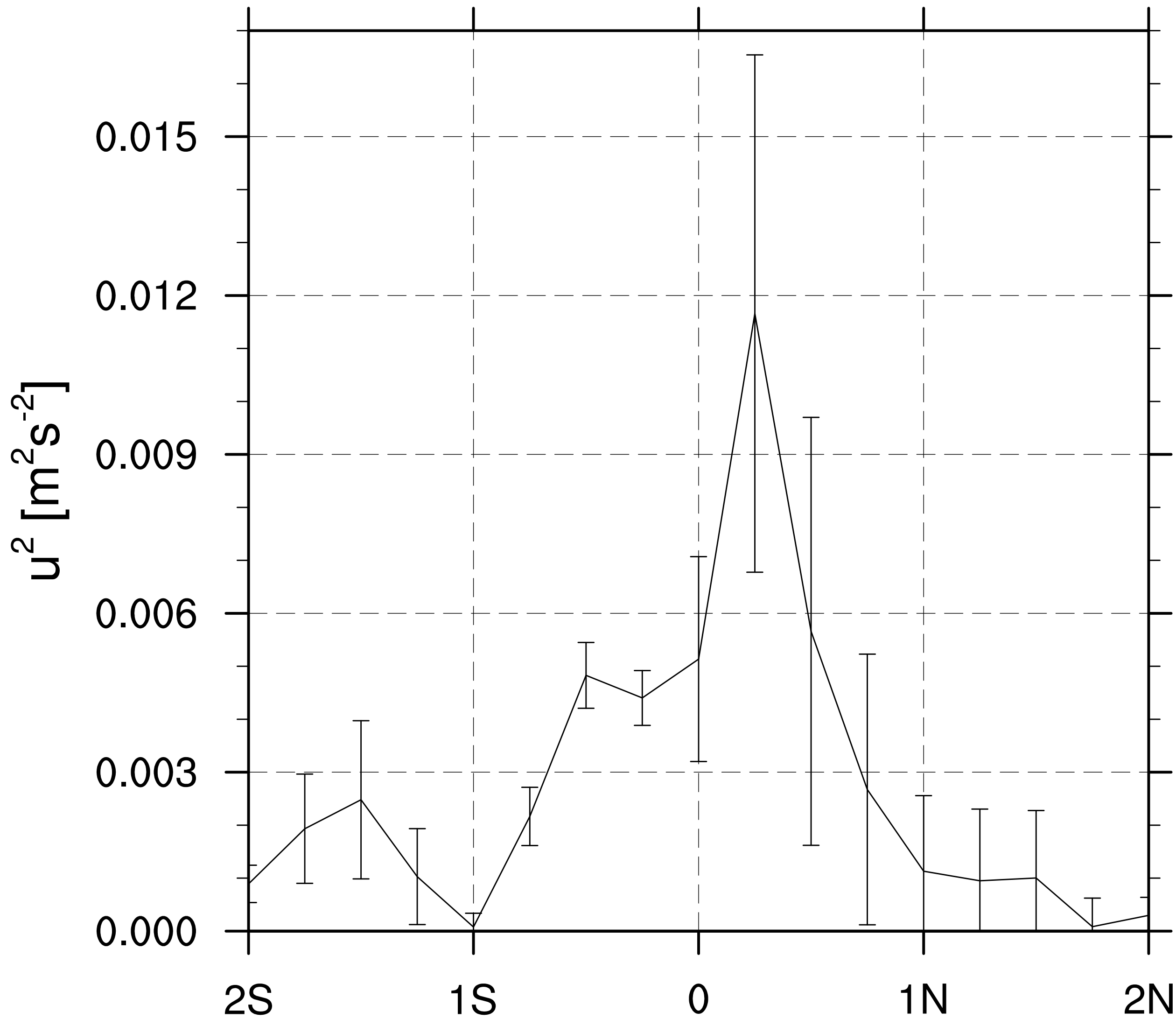

Fig. 5. The amplitude squared of the 1670 day harmonic fit to the zonal velocity from the ARGO float data (parking depth 1000 m) in the longitude band 15°W to 30°W plotted as a function of latitude together with error bars assuming each measurement to be independent. See text for details.

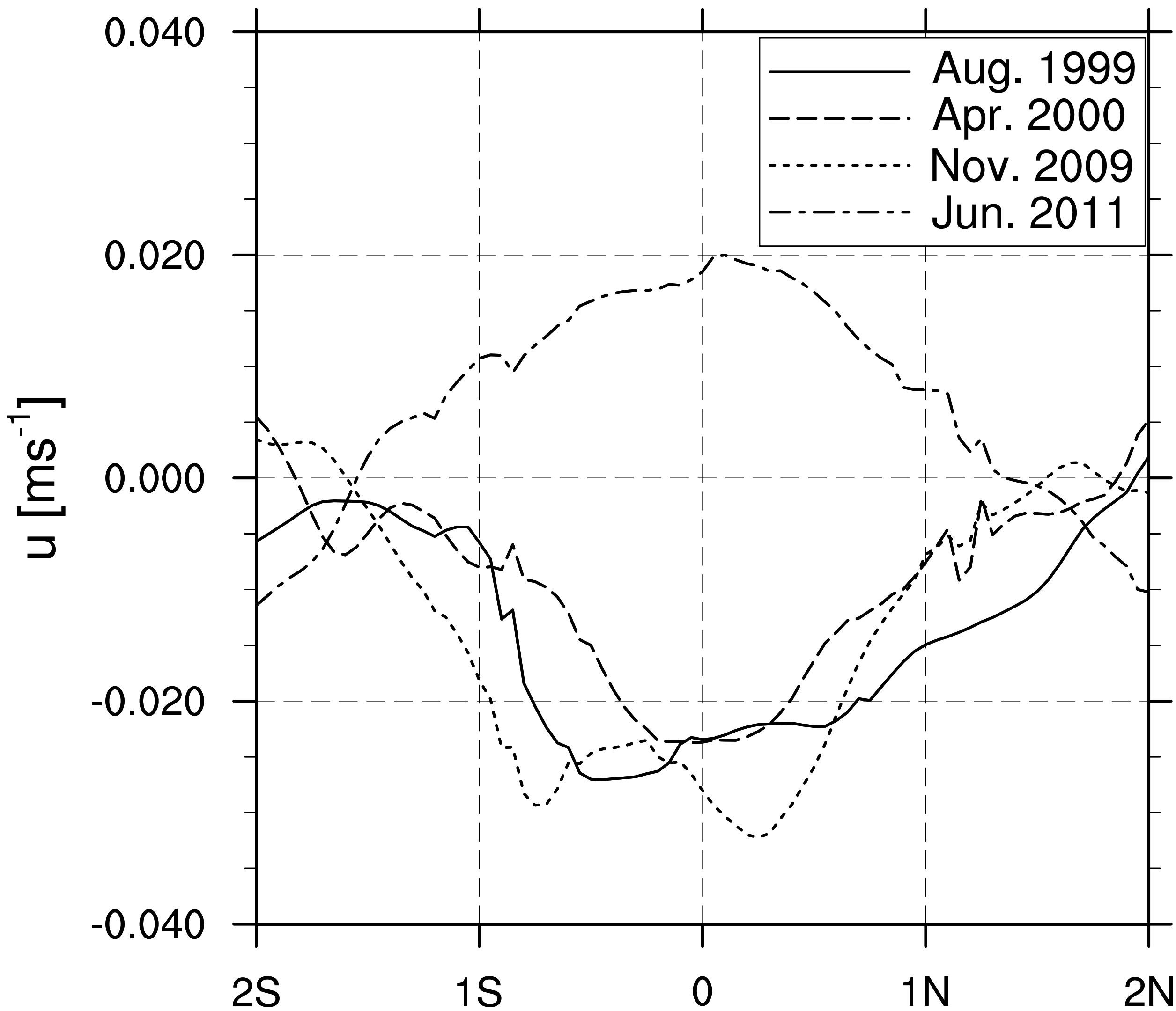

FIG. 6. The projection of the zonal velocity onto the 17th vertical normal mode (corresponding to the equatorial deep jets) from the cruises with data down to 4000 m and deeper listed in Table 1. See text for details.

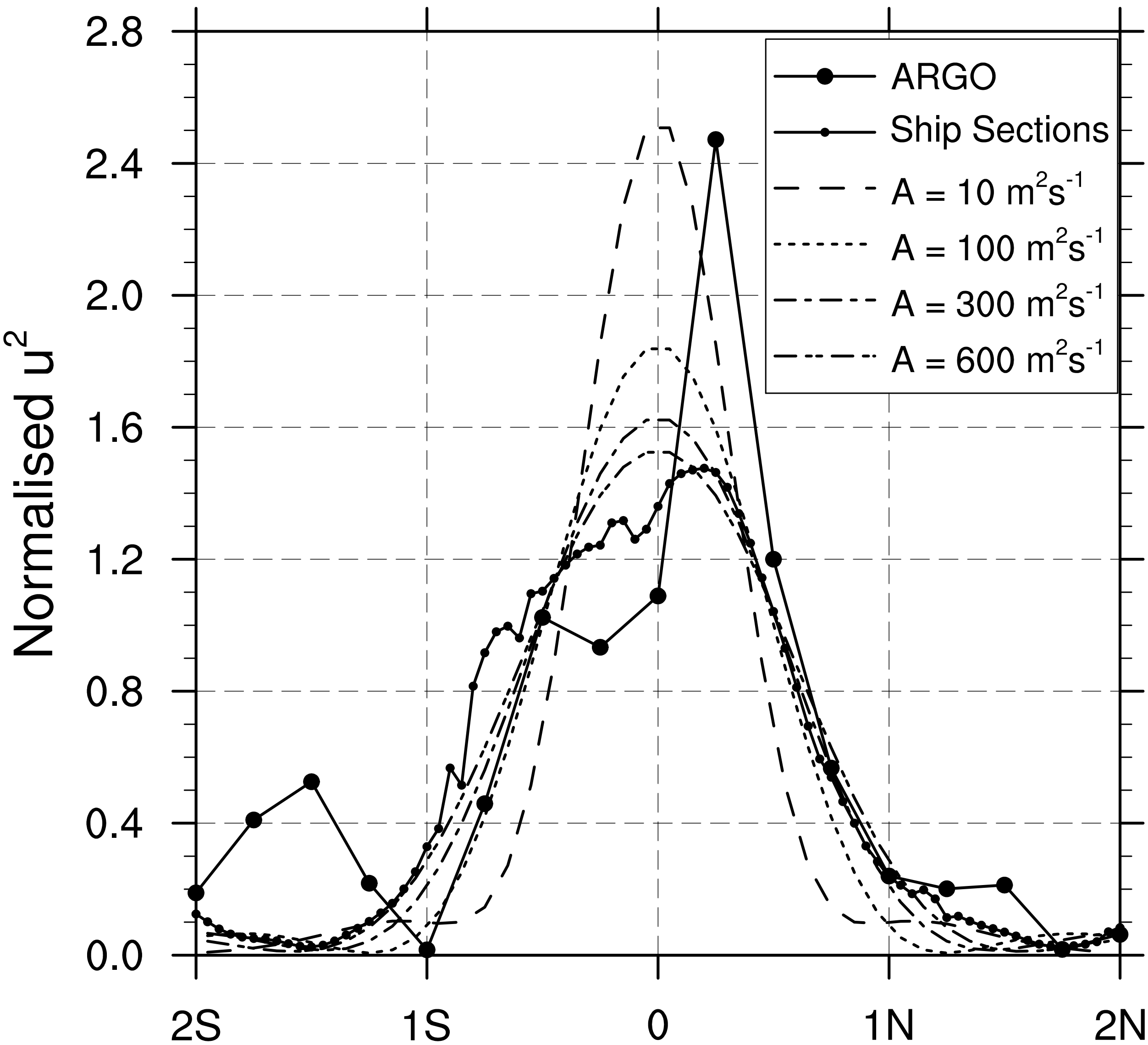

FIG. 7. A comparison between normalised cross-equator profiles of the deep jet zonal velocity squared from the ARGO float data (derived from Figure 5), the ship sections (derived from the zonal velocity projections plotted in Figure 6) and the zonal velocity squared from the model for values of $A = 10$, 100, 300 and 600 m^2 s^{-1} (see text for details).

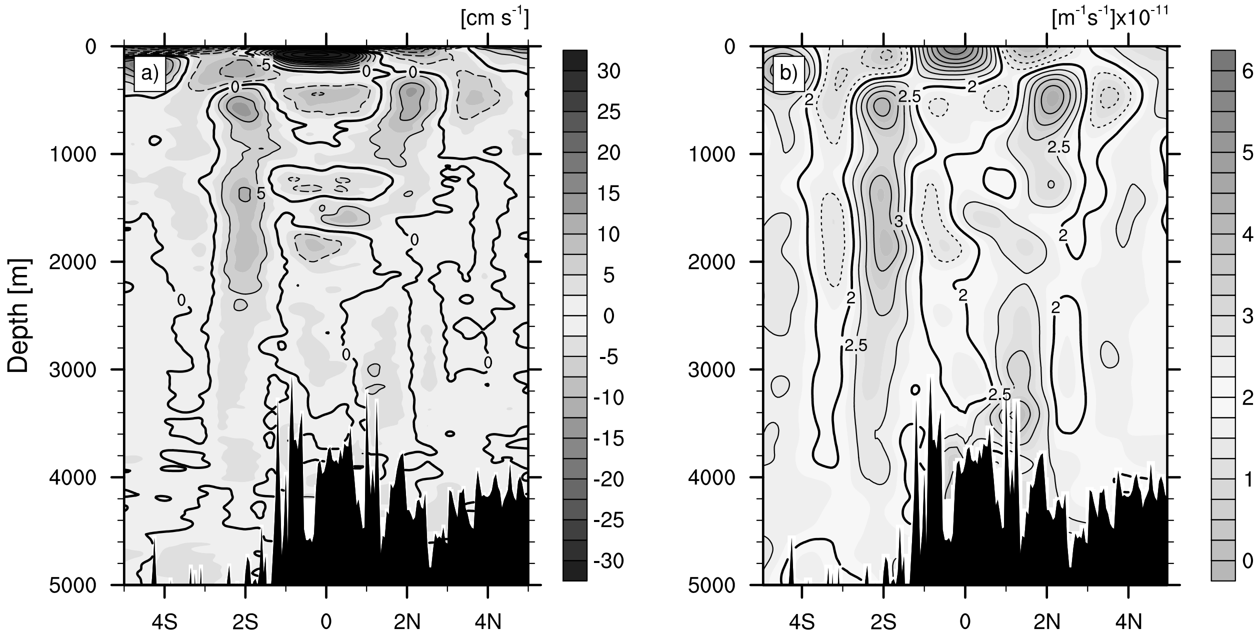

FIG. 8. (a) The mean zonal flow through 23°W derived from the cruises listed in Table 1. Negative values, indicating westward flow, are shown using dashed contours and the contour interval is 0.05 m s^{-1}. (b) The meridional gradient of the absolute vorticity derived from the flow field in (a). The contour interval is 0.5×10^{-11} m^{-1} s^{-1} and dashed contours indicate values below 2×10^{-11} m^{-1} s^{-1} (corresponding roughly to planetary β). In (b) a smoothing has been applied using a Gaussian filter with influence radii of 100 m in the vertical and 0.5° in latitude and cut-off radii of 200 m and 1 degree latitude.